Journal of Biomedical Optics

SPIEDigitalLibrary.org/jbo

In vivo wound healing diagnosis with second harmonic and fluorescence lifetime imaging

Gitanjal Deka
Wei-Wen Wu
Fu-Jen Kao

SPIE

In vivo wound healing diagnosis with second harmonic and fluorescence lifetime imaging

Gitanjal Deka,[a*] Wei-Wen Wu,[a,b*] and Fu-Jen Kao[a]
[a]National Yang-Ming University, Institute of Biophotonics, Taipei 112, Taiwan
[b]Taipei City Hospital, Division of Plastic & Reconstructive Surgery, Department of Surgery, Heping Fuyou Branch, Taipei, Taiwan

Abstract. Skin wounds heal when a series of cell lineages are triggered, followed by collagen deposition, to reconstruct damaged tissues. This study evaluates the regeneration of collagen and change in cellular metabolic rate *in vivo* during wound healing in rats, with second harmonic generation (SHG) and fluorescence lifetime imaging microscopy respectively. The metabolic rate of cells is reflected through the lifetime of the autofluorescence from the co-enzyme protein, reduced nicotinamide adenine dinucleotide, due to its change in the relative concentration of bound and free forms. A higher than normal cellular metabolic rate is observed during the first week of healing, which decreases gradually after eight days of wound formation. SHG signal intensity change indicates the net degradation of collagen during the inflammatory phase, and net regeneration begins on day five. Eventually, the quantity of collagen increases gradually to form a scar tissue as the final product. Importantly, this work demonstrates the feasibility of an *in vivo* imaging approach for a normal wound on rat skin, which has the potential to supplement the noninvasive clinical diagnosis of wounds. [DOI: 10.1117/1.JBO.18.6.061222]

Keywords: fluorescence lifetime imaging microscopy; reduced nicotinamide adenine dinucleotide; second harmonic generation; collagen; wound healing.

Paper 12551SS received Aug. 24, 2012; revised manuscript received Oct. 31, 2012; accepted for publication Nov. 21, 2012; published online Dec. 18, 2012.

1 Introduction

As an important organ for functions such as sensation, insulation, prevention of excessive water loss, and protection of the body from outside pathogens, skin can repair itself through wound healing, if any damage in it occurs. Wound healing involves different phases of cellular activity triggered by specific growth factors and signaling molecules.[1] Initially, skin is repaired temporarily, owing to a fibrin clot that plugs the defects. Over subsequent days, the wound heals completely by forming collagen-rich dynamic scar tissue.[1] Histological studies on wound healing reveal several vital sequential stages in wound repair, such as inflammation, fibroplasias, and capillary invasion into the clot to start the contractile granulation phase. Formation of granulation tissue draws the wound margins together.[2] The sedentary cells proliferate and lay down a bed of connective tissue matrix to fill the wound gap.[1] A wound normally repairs quickly, within two to three weeks. However, the epidermal portions lost at the wound site fail to regenerate, leaving a scar of connective tissue. These scars consist mainly of poorly reconstructed thick parallel bundles of collagens.[3]

Conventionally, wounds are clinically observed with histochemical assessment of the biopsies invasively.[4,5] These methods may interfere with wound healing in terms of activity and metabolic rates of the cells involved.[4–7] Common clinical methods to diagnose wounds are the use of clinical signs,[8] clinical biopsies, and needle aspiration.[9–12] However, some of these methods are limited in nonquantitative and nonqualitative measurements and may even cause further tissue damage and delay healing when biopsies are taken. This study demonstrates the feasibility of using laser-induced noninvasive methods for diagnosing normal wounds.

Since the development of short pulse lasers, optical imaging with nonlinear and multiphoton excitation has emerged as an important microscopy technique.[13–17] Multiphoton modalities have overcome some of the difficulties in autofluorescence spectroscopy based on single photon excitation, including photobleaching,[18,19] photo damage,[20,21] significant light scattering and absorption in tissues.[22,23] Among them, femtosecond Ti:sapphire laser can achieve two photon excitation of nicotinamide adenine dinucleotide (NADH) from an intracellular region and SHG from the collagen of extracellular matrix.[24–27] NADH functions as a coenzyme that donates electrons in the electron transport chain (ETC) of oxidative phosphorylation. Cellular NADH exists in two physiological forms: free and protein bound. Upon binding to mitochondrial membrane proteins, NADH molecules get associated with the energy generation pathway.[28] Therefore, evaluating the ratio between free and enzyme-bound forms of the fluorophore (NADH) can provide further insight into the metabolic state of cells. Free and bound states of NADH have well separated values of fluorescence lifetimes.[29] As NADH binds to a protein, its lifetime increases from ~0.4 to ~2.5 ns.[30–33] By fitting the fluorescence decay of fluorescence lifetime imaging microscopy (FLIM) to a double exponential model, the relative concentration of this coenzyme's functional states (denoted as a_1 and a_2) can be measured.[26] In the extracellular matrix, collagen is the most abundant connective tissue, characterized by optical noncentrosymmetricity.[34] Zoumie et al. in their study of a tissue model have described spectrally resolved imaging of different parts of the

*These authors contributed equally to this work.

Address all correspondence to: Fu-Jen Kao, National Yang-Ming University, Institute of Biophotonics, 155 Linong Street, Section 2 Taipei 11221, Taiwan. Tel: +886 2 28267336; Fax: +886 2 28235460; E-mail: fjkao@ym.edu.tw

0091-3286/2012/$25.00 © 2012 SPIE

skin layers by using a combined two photon excited fluorescence and second harmonic generation technique.[27] Since collagen is a highly nonlinear optical material, studying collagen regeneration with SHG to monitor wound healing is relatively easy as it plays a critical role in healing physiology.[35] Previous works have demonstrated the feasibility of applying SHG microscopy to the morphological features of various tissue models.[36–38] Thus change in collagen intensity and regeneration direction at the healing wound could provide important information for clinical diagnosis.[36,39] Elucidating the femtosecond laser induced second-order nonlinear phenomenon allows us to evaluate rat skin wound healing process, noninvasively, by monitoring the cellular metabolic rate of NADH free to bound ratio change and the collagen regeneration using FLIM and SHG, respectively.

2 Materials and Methods

2.1 *Experimental Design and Sample Preparation*

Five Sprague Dawley (SD) male rats fulfilled the demands of appropriate host for an *in vivo* noninvasive wound healing study. The rats were supplied by the National Yang Ming University Animal Center. The rats were seven weeks old at the beginning of the experiment, with an average weight of 280 g. The experiment was performed in a time lapsed schedule for the wound aging as from after one day, two days, three days, four days, five days, six days, eight days, 10 days, 12 days, 16 days, and 20 days of wound formation. Additionally, the day of wound formation was defined here as the 0'th day. On each rat, a normal skin position was marked [Fig. 1(b)], where the data were collected from normal skin for comparison with the wounded tissue. Next, each of the five rats was sedated intraperitoneally with pentobarbital (pento) sodium (SCI. Pharmatech Inc., Taiwan). A 0.2 molar solution of pento was prepared in 0.9% isotonic saline solution. The rats were injected with a concentration of 50 mg per kg of rat weight. At every 1 h interval, the rats were sedated with the same amount of drug. Three circular wounds with a diameter of 8 mm and a depth of 2 mm on the back of each rat were made with a punch biopsy (Biopsy Punch, Miltex Inc., Pennsylvania 17402).

2.2 *Multiphoton Excitation*

Both FLIM and SHG images were obtained by using a modelocked Ti:sapphire Mira F-900 laser (Coherent, United States), capable of producing 80-MHz femtosecond laser pulses in the spectral range from 700 to 1000 nm, pumped by a solid-state frequency-doubled 532 nm Verdi laser (Coherent, United States) and operating at 740 nm for the two-photon excitation of cellular NADH autofluorescence and collagen second harmonic generation. The excitation beam was coupled to the FV300 (Olympus, Japan) scanning unit as reported previously with the scanning speed set by a function generator (AFG310, New Jersey 07740) to optimize the image acquisition.[40] Figure 2(a) schematically depicts the instrumentation used in this experiment. The laser beam was focused on the wounded tissue with a 20×0.40 numerical aperture (NA) Plan Apochromat air objective (Olympus, Japan). To avoid photo damage of the tissue, an average laser power of ~5.5 mW after the objective was used for imaging. Measurements were conducted on a modified inverted Olympus microscope IX 71 (Olympus, Japan). To match the spectral characteristics of excited molecules, a bandpass filter of 447 ± 30 nm was used for NADH autofluorescence signal and 360 ± 40 nm (Semrock, USA) was used for collagen SHG signal detection, respectively.[41] For rejection of the excitation light at 740 nm, an additional short-pass infra red (IR) cutoff filter was used. Finally, the autofluorescence and second

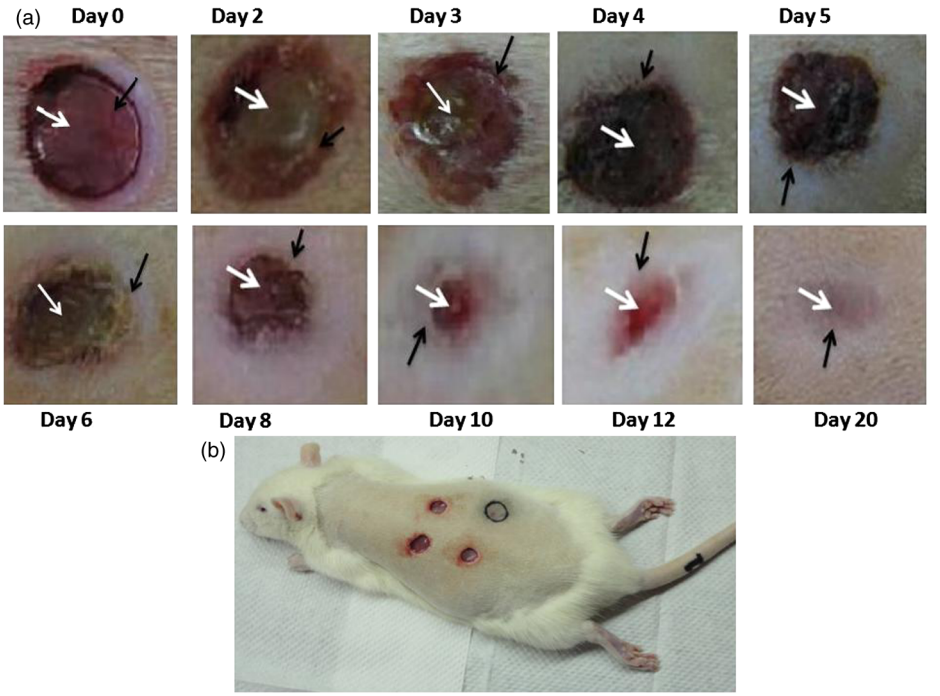

Fig. 1 (a) Digital photograph assessment of healing progression from day 0 to day 20. The white arrow shows one of the positions of data acquisition at center, and the black arrow shows one of the data acquisition spot at edge; (b) representative rat with three wounds on its back with a black circle indicating the portion of the skin that was used in data acquisition for normal skin.

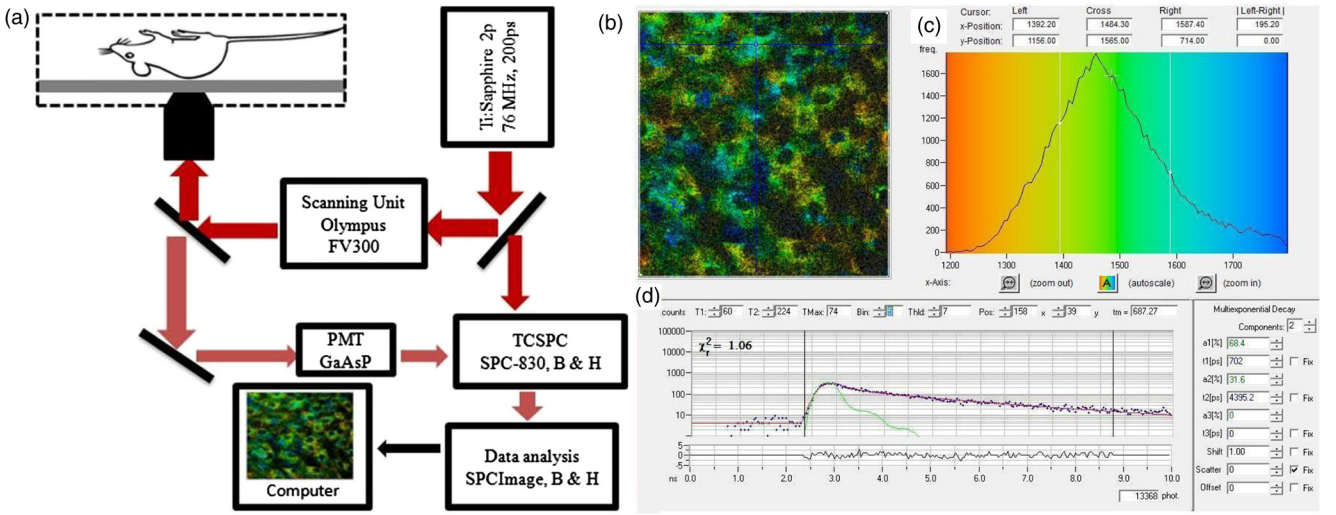

Fig. 2 (a) Schematics of the experimental setup for FLIM and SHG imaging; (b) color-coded image of the cells presents at the dermis of the skin; (c) the distribution curve is the color-coded mean lifetime (tm) distribution curve from the whole frame; (d) the depicted decay curve is from a single pixel of the body of single cell.

harmonic signals were detected by a cooled GaAsP PMT (H7422-P40, Hamamatsu Photonics Hamamatsu, Japan).

2.3 *Photon Acquisition*

The acquisition of SHG from collagens and cellular NADH's FLIM data were acquired by a time-correlated single photon counting system (TCSPC) (SPC-830, Becker & Hickl, GmbH, Germany).[42,43] Since SHG is a scattering process, the lifetime shown by the SHG signal is comparable to just the instrumental response of the system. All FLIM images were taken at 256 × 256 pixels resolution with the accumulation time of 800 s for gathering sufficient photon counts for statistical data analysis.

2.4 *Data Analysis*

Data were analyzed using SPCImage (v. 2.8) software (Becker & Hickl, GmbH, Germany).[44] Lifetime calculation from the multiexponential decay was done by mathematical convolution of a model function and the instrument response function (IRF) by fitting with the experimental data. Lifetimes from the composite decays of NADH were then derived by convolution of an IRF, I_{instr}, with a double-exponential model function, defined in Eq. (1), with offset correction for the ambient light and/or dark noise I_0 to obtain calculated lifetime decay function $I_c(t)$ in Eq. (2)

$$F(t) = a_1 e^{-t/\tau_1} + a_2 e^{-t/\tau_2}, \tag{1}$$

$$I_c(t) = \int_{-\infty}^{\infty} I_{\text{instru}}(t)[I_o + F(t)]\mathrm{d}t, \tag{2}$$

where $a_1 e^{-t/\tau_1}$ and $a_2 e^{-t/\tau_2}$ denote the contributed fluorescence decays from short and long lifetime components of NADH, respectively; τ_1 and τ_2 represent their corresponding lifetime constants; and a_1 and a_2 refer to the corresponding relative amplitudes. Figure 2(b) shows an example of the SPCImage software window with the color-coded FLIM image of average lifetime (τ_m), the color-coded lifetime distribution histograms [Fig. 2(c)], below which the photon decay curve from the wounded tissue is also depicted [Fig. 2(d)]. Next, I_{instr} was measured experimentally with the periodically poled lithium niobate (PPLN) crystal at 370 nm for NADH imaging (i.e., the second harmonic of 740 nm from the Ti:Sapphire laser). The decay full-width-half-maximum thus obtained was equivalent to ~320 ps. The average lifetime was calculated as an amplitude-weighted parameter of the two lifetime components:

$$\tau_m \equiv \frac{a_1\tau_1 + a_2\tau_2}{a_1 + a_2}. \tag{3}$$

The model parameters (i.e., a_i and τ_i) were derived by fitting the decay $I_c(t)$, from Eq. (2), to the actual data $I_a(t)$ by minimizing the goodness-of-fit function defined in Eq. (3), using the Levenberg-Marquardt search algorithm,

$$\chi_R^2 = \left\{\sum_{k=0}^{n} [I_a(t) - I_c(t)]^2 / I_a(t)\right\} \Big/ (n-p), \tag{3a}$$

where n denotes the number of data (time) points (equal to 256), and p represents the number of model parameters. The ratio of a_1 and a_2 is the best indicator of free and protein-bound states of NADH, which can be used to depict the status and changes in cellular metabolism.[26] Note that higher value of a_2 represents higher fraction of protein-bound NADH. Thus the value of a_1/a_2 ratio is inversely proportion to the metabolic activity.

2.5 *SHG Intensity Measurements*

The second harmonic images were analyzed for SHG signal intensity by using the Java-based image-processing program Image-J (National Institute of Health, USA). The SHG images from the five rats (total 15 wounds) were averaged, and then the normalized intensities were plotted against the time course in days. The photon counts were obtained using the SPCImage software (Becker & Hickl, GmbH, Germany).

2.6 *Digital Camera Images*

For normal observation of the healing progression, digital camera images were obtained using a Canon Power shot 10-D digital camera (Canon, U.S.A.) (Fig. 1).

3 Results

3.1 *Cellular Metabolic Perturbation at Different Stages of Wound Healing*

Perturbation in the metabolic rate of the cells involved at the wound site was detected by monitoring the NADH free to protein bound ratio change.[45] The entire epidermal and upper dermal layers of the skin were removed at the time of wounding. Upon imaging, cellular autofluorescence from the wound was not observed on the day of wound formation. Figure 3(a) illustrates the scatter chart diagram of NADH a_1/a_2 change with the wound healing progression (Note: the value of a_1/a_2 ratio is inversely proportion to the metabolic activity). This figure revealed a higher metabolic rate from day first to sixth with averaged peak value of a_1/a_2 distribution (the peak value of the a_1/a_2 distribution histogram averaged for 15 wounds) within the range of 1.8 to 2 at the center. From the eighth day, the metabolic rate gradually decreased, where the a_1/a_2 value reaches 2.2 on that day. From the tenth day to twentieth, the ratio increased gradually within a range of 2.4 to 3.5 [Fig. 3(a)]. Since wound healing is mainly triggered and operated by the cells at the edge, the cellular metabolic rate at the edge was compared with the center [Fig. 3(a)]. Moreover, the wound healed from the edge, finally reaching the center. Owing to that, while data was taken for the edge, the imaging position was moved toward the center on each day as the healing progressed. Figure 1(a) displays one of the positions of laser irradiation at the edge (black arrows) and center (white arrows) in order to acquire data. The metabolic rate at the edge was high and comparable with that of the center for the first three days. From the fourth day, the cellular activity decreased at the edge and the average value of a_1/a_2 increased to 2.5 in comparison to center, 2.1. The average free to protein bound NADH ratio at the edge was approximately same from the fourth to tenth day within a range of 2.35 to 2.65. Before the fourth day, the edge of the wound was also under inflammation [Fig. 1(a)], subsequently causing a comparable metabolic rate of edge with that of center. According to our results, newly generated skin appeared at the edge, starting from the fourth day [Fig. 1(a)] and subsequently decreasing cellular metabolism due to complete healing. Additionally, the area of newly formed skin increased toward the center with each passing day, finally reaching the center

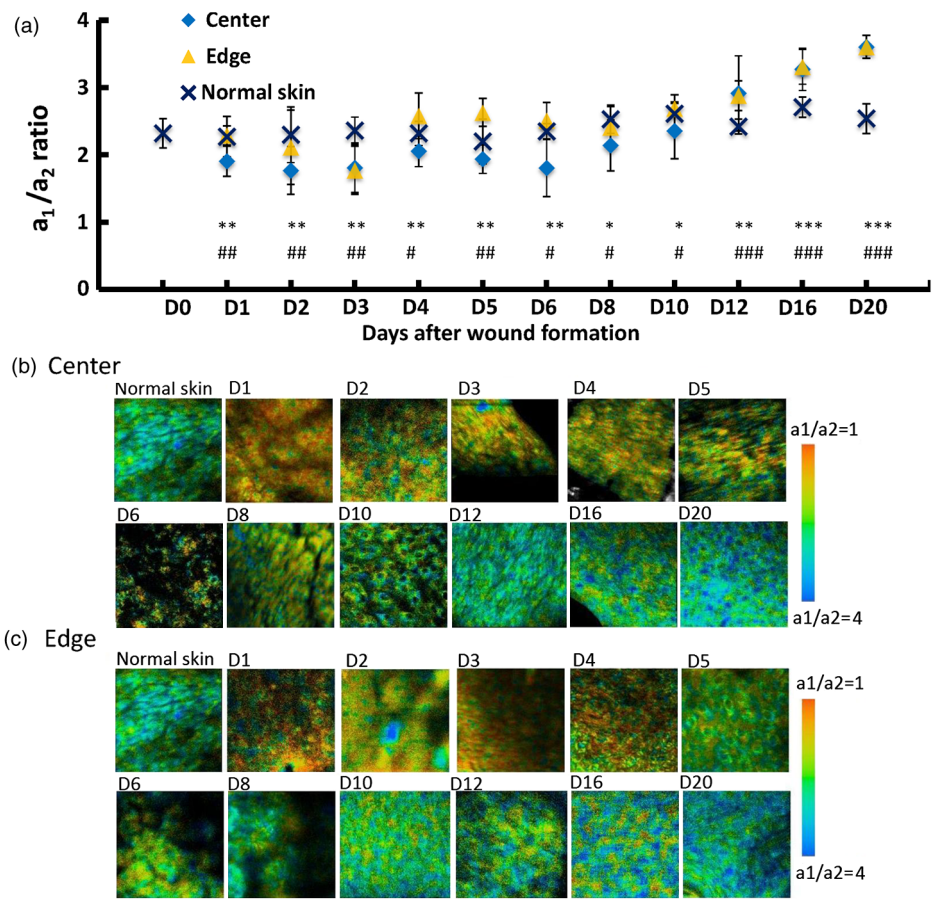

Fig. 3 (a) Scatter chart diagram of day by day assessment of peak values of NADH a_1/a_2 distribution, averaged over 15 wounds at each days of wound observation, here "D" represents "day." The error bars represent the standard error of the mean for a_1/a_2 ratio measurement. Statistical significance of the experimental results was evaluated by two-side Student's t-test. Significant differences of a_1/a_2 values at center from normal skin are indicated by *: $P > 0.05$, **: $0.05 > P > 0.001$, and ***: $P < 0.001$. The significant differences of a_1/a_2 values at edge from normal skin are designated as #: $P > 0.05$, ##: $0.05 > P > 0.001$, and ###: $P < 0.001$. P value less than 0.05 was considered significant; (b) representative color-coded FLIM images of a_1/a_2 ratio of NADH at the wound center; (c) representative color-coded FLIM images of a_1/a_2 ratio of NADH at the wound edge.

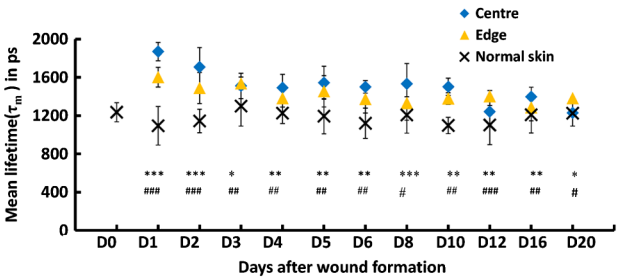

Fig. 4 Scatter chart diagram of day by day assessment of peak values of NADH mean lifetime (τ_m) distribution, averaged over 15 wounds at each days of wound observation, here "D" represents "day." The error bars represent the standard error of the mean for the τ_m measurement. Statistical significance of the experimental results was evaluated by two-side Student's t-test. Significant differences of τ_m values at center from normal skin are indicated by *: $P > 0.05$, **: $0.05 > P > 0.0501$, and ***: $P < 0.001$. The significant differences of τ_m values at edge from normal skin are designated as #: $P > 0.05$, ##: $0.05 > P > 0.01$, and ###: $P < 0.001$. P value less than 0.05 was considered significant.

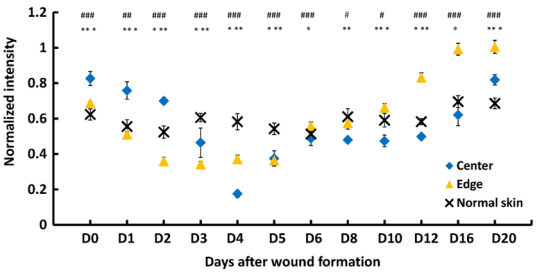

Fig. 5 Time-lapsed regeneration of collagen depicted in normalized SHG intensity scatter plot with respect to the maximum intensity observed at the edge on day 20. The error bar represents the standard errors of the mean for the SHG intensity measurements, here "D" represents "day." Statistical significance of the experimental results was evaluated by two-side Student's t-test. Significant differences of SHG intensity at center from normal skin are indicated by *: $P > 0.05$, **: $0.05 > P > 0.001$, and ***: $P < 0.001$ for center. The significant differences of SHG intensity values at edge from normal skin are designated as #: $P > 0.05$, ##: $0.05 > P > 0.001$, and ###: $P < 0.001$. P value less than 0.05 was considered significant.

[Fig. 1(a)]. Thus the free to protein-bound NADH ratio value was increased even more, starting from the tenth to the twentieth day. As the entire wound started to acquire new skin after a week, similar values of a_1/a_2 ratio at the center and edge were measured, starting from the tenth day. Color-coded FLIM images in Fig. 3(b) and 3(c) illustrate the relative increase of free form NADH over bound form during the healing process at the center and edge, respectively.

The mean fluorescence lifetime (τ_m) of the two components is also a marker of the state of cellular microenvironment. Free and protein-bound components of NADH had peaks for fluorescence lifetimes (τ_1 and τ_2), averaged at 550 and 3100 ps, respectively. These results are close to previously reported values.[46,47] The observed mean lifetime (τ_m) one day after wound formation was higher than all other days after that. The mean lifetime decreased linearly as the wound healed. On the first two days, the τ_m value at center was higher than the edge; however, from the third onward, the values were nearly the same for both the center and edge. On the first and second days, average mean lifetimes were 1870 and 1700 ps at the center and edge, respectively (Fig. 4). From the third day, the τ_m value from the center and edge fell below 1500 ps and gradually decreased. As the wound healed fully on the twentieth day, the values resembled those found in normal skin (Fig. 4). This change in mean lifetime during the healing process may be attributed to the different degrees of NADH binding to the mitochondrial membrane protein relative to the unbound NADH and the cellular microenvironmental change for the coenzyme (NADH).

3.2 *Delayed Healing Due to Degradation and Regeneration of Collagen*

This study also evaluated the collagen SHG intensity from the wounded tissue. Figure 5 illustrates the histogram of change in normalized SHG intensity, with the healing progression, from the surface of the wounded center and edge. This figure revealed a higher SHG signal from the dermis layer left at the wounded center on the day of wound formation owing to the directly exposed dermal collagen. For normal skin, the image at 250 μm deep inside the tissue from the dermis layer was taken each day within the blacked marked area [Fig. 1(b)]. After wound formation the SHG images from collagens were taken only from the exposed surfaces, within a range of 0 to 5 μm in Z-direction (perpendicular to the wound surface), where new collagens were laid. Our results further indicated a lower intensity after 24 h of wounding; that intensity decreased more on the second and third days at the center of the wound and reached least value on the fourth day (Fig. 5). Although the SHG signal was low, on the fifth day, the signal value started to increase (Fig. 5). After the sixth day, the signal intensity increased three times more than that on the fourth day, and remained nearly the same up to the twelfth day. Collagen generation was detected in a higher amount after the twelfth to twentieth days, which was required for the observed scar formation (Fig. 5). On the twentieth day, an even higher SHG intensity than that of a normal skin was observed. At edge of the wound, the SHG signal was higher than that of the center (Fig. 5). Also at the edge, although the SHG signal decreased in the first three days, the intensity was higher in value than in the center (Fig. 5). After the fourth day, the signal improved more at the edge than in the center as newly generated skin began to appear at the edge first [Fig. 1(a)]. Although comparatively same SHG signal was observed on the fifth and sixth day, the deposition of collagen at the edge outnumbered that of the center from the eighth day onward. The detected SHG signal intensity differences between center and edge were increasingly smaller on day sixteenth and twentieth than that on the twelfth day. This finding suggests that, when the wound undergoes the remodeling phase, collagens deposit in a greater amount as the days passes by; in addition, it is expected to further increase the SHG intensity at the center.

3.3 *Enhanced Alignment of Regenerated Collagens in the Scar than in the Normal Skin*

This study also compares the qualitative collagen regeneration with the healing process (Fig. 6). A random organization of collagen bundles were observed from the normal skin. From the first to third day, the collagens were clearly observed with the SHG signal (Fig. 6). Native collagens were found on the exposed dermis of the wound, when the upper epidermal and a portion of the dermal layer were removed. No autofluorescence was observed on the day of wound formation, due to the removal of the epidermal layer of the skin containing cells. The autofluorescence signals detected on the first to third day originated from the blood and tissue fluid containing inflammatory and

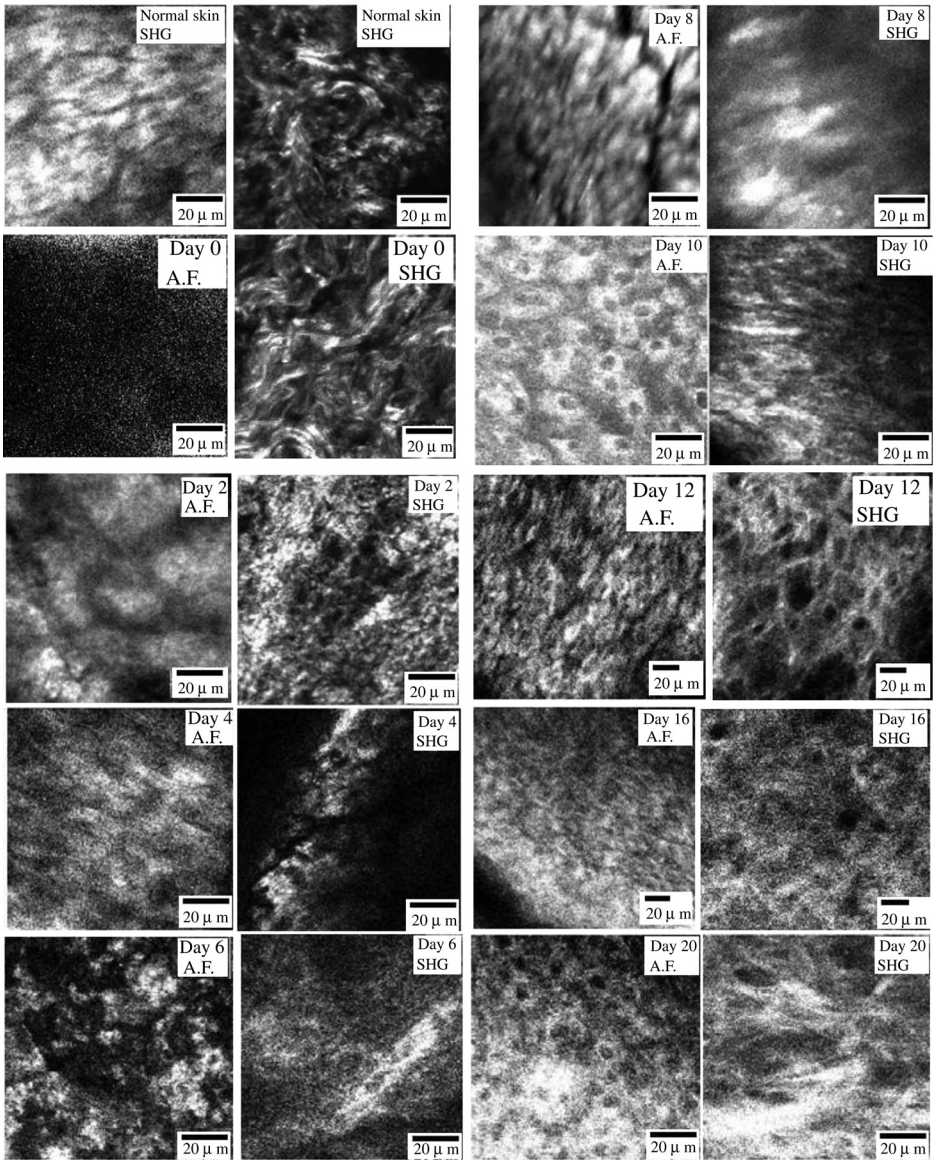

Fig. 6 Cellular NADH autofluorescence intensity images compared with the SHG images from the same laser spot. It was not easy to select exactly the same spot for the imaging on each day, but it was kept on mind to choose the same region of interest on each day of observation.

blood cells that were not easily resolved. On fourth day, the observed collagens were in a nonfibrillar form (Fig. 6). Additionally, without the help of an infrared exciting laser, acquiring SHG signals from the wound site was rather difficult due to the formation of the opaque fibrin clot during this phase. Although this decrease in intensity slightly improved on the sixth day, fibrous collagen was not observed until tenth day (Fig. 6). As the skin layers began to regenerate, the cells also begun to appear from the eighth day on the NADH autofluorescence images. Ultimately, on the twentieth day of healing, well-organized fibrillar collagens and cells were observed on the newly form scar tissue (Fig. 6).

4 Discussion

Wound healing comprises of sequential changes in different cell initiation, activation and migration events. Those changes are categorized into different, yet overlapping, phases: (1) hemostasis; (2) inflammatory; (3) proliferative; and (4) remodeling.[48,49] This study has demonstrated the feasibility of an optical microscopy-based noninvasive approach, capable of providing insight into these sequential phases in terms of cellular activity and collagen regeneration independently. Negligible concentration of cells relative to the extra-cellular matrix (ECM) at the exposed dermal layer prohibit us from detecting significant cellular autofluorescence on the day of wound formation that can be used for statistical lifetime fitting.[50] The higher metabolism observed both at the center and the edge of the wound, from the first to third day indicates the execution of the inflammatory response by the neutrophils and monocytes sequentially to clean the wound site by phagocytise the debris, bacteria and the damage tissue.[1,51,52] The initiation of granulation phase, by fibroblast and epidermal cell migration to the center of the wound, maintained the metabolism higher after the third to sixth day of wound formation and was comparable to the first three days.[53,54] However, the wounded edge healed faster than the center, and the phases of healing were also of shorter duration. Previously, Stedelmann et al. found that in the first two or three days after injury, fibroblasts migrate and proliferate. Meanwhile, after a

week, they are the main cells that lay down the collagen matrix in the wound site.[48] Approximately a week after wounding, contraction begins in the wound, as fibroblasts had differentiated into myofibroblasts.[55] When the actins in myofibroblasts contracts, the wound edges are pulled together.[55] Fibroblasts lay down collagen to reinforce the wound as the myofibroblasts contract.[48] The cellular metabolic rate was observed to have decreased both at the center and edge after the tenth day. This state of lower cellular activity appears at the edge earlier than at the center, as the edge heals faster than the center due to greater access to the nourishment and growth factors from the undamaged tissues. The mean lifetime (τ_m) of wounded tissues was more diverse than that of the normal skin during first few days of wound healing, but it gradually becomes similar to the normal one as it heals. Observed mean lifetime change indicates that in healed tissue, the micro environmental difference within the cell was negligible in comparison to the normal skin cells. But during the first few days of wound healing the microenvironment within the cell was different in terms of viscosity, pH and temperature that reflect cellular mobility, enzymatic reactions and inflammation respectively.[46] During the first three days, collagens were observed in the exposed dermis and were degraded by the metalloproteinase enzymes secreted by the migrating epidermal cells at the wound bottom. However, as time proceeds, regeneration exceeded the degradation, and a newly laid matrix of collagen was formed gradually to fill up the wound gap, which was detected by the increase in SHG signal intensity (Fig. 5). The collagen regeneration started earlier at the edge than the center, and it remained higher throughout the process owing to its direct communication with the undamaged tissues. The collagens are deposited in the wound until the gap is filled, and the wound enters into the remodeling phase, which can last from weeks to several months. The remodeling phase is a slow process, which does not require high cellular activity. During this process, the older collagens are replaced by young and stronger ones to strengthen the wound.[56] Originally disorganized collagen fibers are rearranged, cross-linked, and aligned,[57] which can be observed from the images of (Fig. 6). Briefly our results indicate that at the initial phase of wound healing the metabolic rate of cells was higher, which was caused by the activated cells due to inflammation and initial cell migration. At the edge wound heals faster, which was reflected by the decrease in metabolic rate than that of center and was comparable to normal skin after three days. After eight days, new skin regenerates at the center too, and the metabolic rate becomes comparable to normal skin. But as the healing completed, the regenerated new skin forms a scar mainly comprised of collagen, which is differing from the normal skin in terms of strength and physiology. Our result indicates lower cellular activity in scar tissue than that of normal skin.

Although cellular metabolic changes are related to collagen regeneration, correlating them in this study would be inappropriate. Since many cell types are immobilized during the healing process, the NADH autofluorescence signal fails to differentiate the fibroblast cells among them. As is well known, collagens are laid by the fibroblasts, explaining the difficulty in this study to establish a correlation between the collagen regeneration and fibroblast metabolism.

5 Summary

FLIM of cellular NADH can characterize the physiological status of cells in tissues by monitoring the cellular metabolic rate. In skin tissue regeneration, collagens are also crucial biomolecules that can be mapped by SHG. This study has demonstrated the feasibility of studying wound healing physiology noninvasively. Experimental results indicate that the cellular metabolic rate is higher on the first week at the center and first three days at the edge than during other times of the healing process. As the wound heals, the metabolic rate decreases. Wound heals from the edge and reaches center at the end. Correspondingly, the metabolism also decreases at the edge first and finally becomes similar to the center at the completely regenerated new skin. Additionally, the delayed healing of wound due to the degradation of native collagens and the regeneration of new collagen is elucidated by using SHG optical methods. Collagens in the newly generated skin are observed to be more aligned than those in normal skin. This noninvasive study of wound healing process, based on collagen regeneration and variation in the cellular metabolic rate, is comparable with that measured clinically through histochemical analysis by other studies.[16,51] Further advances in related techniques and enhanced statistical study may offer improved potential diagnostic supplements to wound healing disorders in chronic and burn wounds. Importantly, the noninvasive ability of multimodal nonlinear microscopy will significantly contribute to the efforts of clinicians to diagnose patient injuries by using a much simpler and painless method.

Acknowledgments

The authors would like to thank the National Science Council of the Republic of China, Taiwan (Contract Nos. NSC99-2627-M-010-002, NSC98-2627-M-010-006, and NSC98-2112-M-010-001-MY3) for financially supporting this research. The Taiwan Mouse Clinic, which is funded by the National Research Program for Biopharmaceuticals (NRPB) of the National Science Council (NSC) of the Republic of China, Taiwan, is appreciated for its technical support. Professor T. B. J. Kuo, Department of Brain Research, National Yang Ming University, is commended for use of his laboratory equipment and space for harvesting and dealing with live rats. Ted Knoy is appreciated for his editorial assistance.

References

1. P. Martin, "Wound healing–aiming for perfect skin regeneration," *Science* **276**(5309), 75–81 (1997).
2. B. Eckes, "Collagen and the reestablishment of dermal integrity," Chapter 16 in *The Molecular and Cellular Biology of Wound Repair*, R. A. F. Clark, Ed., pp. 493–512, Plenum Press, New York (1996).
3. T. L. Tuan et al., "The molecular basis of keloid and hypertrophic scar formation," *Mol. Med. Today* **4**(1), 19–24 (1998).
4. R. J. Snyder, "Treatment of nonhealing ulcers with allografts," *Clin. Dermatol.* **23**(4), 388–395 (2005).
5. J. E. Taylor et al., "Extent of iron pick-up in deforoxamine-coupled polyurethane materials for therapy of chronic wounds," *Biomaterials* **26**(30), 6024–6033 (2005).
6. J. V. Edwards et al., "*In vitro* inhibition of human neutrophil elastase by oleic acid albumin formulations from derivatized cotton wound dressings," *Int. J. Pharm.* **284**(1–2), 1–12 (2004).
7. U. Schönfelder et al., "Influence of selected wound dressings on PMN elastase in chronic wound fluid and their antioxidative potential *in vitro*," *Biomaterials* **26**(33), 6664–6673 (2005).
8. S. E. Gardner et al., "A tool to assess clinical signs and symptoms of localized infection in chronic wounds: development and reliability," *Ostomy. Wound Manag.* **47**(1), 40–47 (2001).
9. G. Dow et al., "Infection in chronic wounds: controversies in diagnosis and treatment," *Ostomy. Wound Manag.* **45**(8), 23–40 (1999).

10. L. Brentano and D. L. Gravens, "A method for the quantification of bacteria in burn wounds," *Appl. Microbiol.* **15**(3), 670–671 (1967).
11. N. S. Levine et al., "The quantitive swab culture and smear: a quick, simple method for determining the number for determining the number of viable aerobic bacteria on open wound," *J. Trauma* **16**(2), 89–94 (1976).
12. F. L. Sapico et al., "The infected foot of the diabetic patient: quantitative microbiology and analysis of clinical feature," *Clin. Infect. Dis.* **6**(Supplement 1), S171–S176 (1984).
13. R. Gauderon et al., "Simultaneous multichannel nonlinear imaging: combined two-photon excited fluorescence and second-harmonic generation microscopy," *Micron* **32**(7), 685–689 (2001).
14. K. Lin et al., "Integrated autofluorescence endoscopic imaging and point-wise spectroscopy for real-time *in vivo* tissue measurements," *J. Biomed. Opt.* **15**(4), 040507 (2010).
15. C. J. R. Sheppard and R. Kompfner, "Resonant scanning optical microscope," *Appl. Opt.* **17**(18), 2879–2882 (1978).
16. Y. Sun et al., "Investigating protein-protein interactions in living cells using fluorescence lifetime imaging microscopy," *Nat. Protoc.* **6**(9), 1324–1340 (2011).
17. W. Denk et al., "Two-photon laser scanning fluorescence microscopy," *Science* **248**(4951), 73–76 (1990).
18. G. H. Patterson and D. W. Piston, "Photobleaching in two-photon excitation microscopy," *Biophys J.* **78**(4), 2159–2162 (2000).
19. L. M. Tiede and M. G. Nichols, "Photobleaching of reduced nicotinamide adenine dinucleotide and the development of highly fluorescent lesions in rat basophilic leukemia cells during multiphoton microscopy," *Photochem. Photobiol.* **82**(3), 656–664 (2006).
20. K. Konig et al., "Pulse-length dependence of cellular response to intense near-infrared laser pulses in multiphoton microscopes," *Opt. Lett.* **24**(2), 113–115 (1999).
21. I. H. Chen et al., "Wavelength dependent damage in biological multiphoton confocal microscopy: a micro-spectroscopic comparison between femtosecond Ti:sapphire and Cr:forsterite laser sources" *Opt. Quant. Electron.* **34**(12), 1251–1266 (2002).
22. A. Schonle and S. W. Hell, "Heating by absorption in the focus of an objective lens," *Opt. Lett.* **23**(5), 325–327 (1998).
23. J. A. Conchello and J. W. Lichtman, "Optical sectioning microscopy," *Nat. Methods.* **2**(12), 920–931 (2005).
24. D. Li et al., "Time-resolved spectroscopic imaging reveals the fundamentals of cellular NADH fluorescence," *Opt. Lett.* **33**(20), 2365–2367 (2008).
25. W. Zheng et al., "Diagnostic value of nonlinear optical signals from collagen matrix in the detection of epithelial precancer," *Opt. Lett.* **36**(18), 3620–3622 (2011).
26. V. V. Ghukasya and F. J. Kao, "Monitoring cellular metabolism with fluorescence lifetime of reduced nicotinamide adenine dinucleotide," *J. Phys. Chem. C* **113**(27), 11532–11540 (2009).
27. A. Zoumi et al., "Imaging cells and extracellular matrix *in vivo* by using second harmonic generation and two photon excited fluorescence," *Proc. Natl. Acad. Sci.* **99**(17), 11014–11019 (2002).
28. M. Cox et al., "Cell chemistry and biosynthesis," Chapter 2 in *Molecular Biology of the Cell*, B. Alberts et al., Eds., pp. 45–124, Garland Science, New York (2008).
29. A. J. W. G. Visser and A. V. Hoek, "The fluorescence decay of reduced nicotinamide in aqueous solution after excitation with a UV-mode locked laser," *J. Photochem. Photobiol.* **33**(1), 35–41 (1980).
30. W. R. Zipfel et al., "Nonlinear magic: multiphoton microscopy in the biosciences," *Nat. Biotechnol.* **21**(11), 1369–1377 (2003).
31. A. Gafni and L. Brand, "Fluorescence decay studies of reduced nicotinamide adenine dinucleotide in solution and bound to liver alcohol dehydrogenase," *Biochemistry* **15**(15), 3165–3171 (1976).
32. M. Wakita et al., "Some characteristics of the fluorescence lifetime of reduced pyridine nucleotides in isolated mitochondria, isolated hepatocytes, and perfused rat liver *in situ*," *J. Biochem.* **118**(6), 1151–1160 (1995).
33. F. Frischknecht et al., "Imaging today's infectious animalcules," *Curr. Opin. Microbiol.* **9**(3), 297–306 (2006).
34. M. Rebecca et al., "Interpreting second-harmonic generation images of collagen I fibrils," *Biophys. J.* **88**(2), 1377–1386 (2005).
35. Z. Ruszczak, "Effect of collagen matrices on dermal wound healing," *Adv. Drug. Deliv. Rev.* **55**(12) 1595–1611 (2003).
36. H. Sorg et al., "Intravital insights in skin wound healing using the mouse dorsal skin fold chamber," *J. Anat.* **211**(6), 810–818 (2007).
37. B. A. Torkian et al., "Modeling aberrant wound healing using tissue-engineered skin constructs and multiphoton microscopy," *Arch. Facial. Plast. Surg.* **6**(3), 180–187 (2004).
38. S. R. Beanes et al., "Confocal microscopic analysis of scarless repair in the fetal rat: defining the transition," *Plast. Reconstr. Surg.* **109**(1), 160–170 (2002).
39. T. Luo et al., "Visualization of collagen regeneration in mouse dorsal skin using second harmonic generation microscopy," *Laser. Phys.* **19**(3), 478–482 (2009).
40. V. Ghukasyan et al., "Application of fluorescence resonance energy transfer resolved by fluorescence lifetime imaging microscopy for the detection of enterovirus 71 infection in cells," *J. Biomed. Opt.* **12**(2) 024016 (2007).
41. S. Huang et al., "Two photon fluorescence spectroscopy and microscopy of NADH(P)H and flavoprotien," *Biophys J.* **82**(5), 2811–2825 (2002).
42. W. Becker et al., "Fluorescence lifetime images and correlation spectra obtained by multidimensional TCSPC," *Proc SPIE* **5700**, 144–151 (2005).
43. W. Becker, "Application of modern TCSPC techniques," Chapter 5 in *Advanced Time-correlated Single Photon Counting Techniques*, W. Becker, Ed., pp. 61–211, Springer, Berlin (2005).
44. V. Ghukasyan et al., "Fluorescence lifetime dynamics of enhanced green fluorescent protein in protein aggregates with expanded polyglutammine," *J. Biomed. Opt.* **15**(1), 016008 (2010).
45. M. C. Skala et al., " *In vivo* multiphoton microscopy of NADH and FAD redox states, fluorescence lifetimes, and cellular morphology in precancerous epithelia," *Proc. Natl. Acad. Sci.* **104**(49), 19494–19499 (2007).
46. J. R. Lakowicz, *Principles of Fluorescence Spectroscopy*, Plenum Press, New York (1999).
47. H. Schneckenburger et al., "Autofluorescence lifetime imaging of cultivated cells using a UV picosecond laser diode," *J. Fluoresc.* **14**(5), 649–654 (2004).
48. W. K. Stadelmann et al., "Physiology and healing dynamics of chronic cutaneous wounds," *Am. J. Surg.* **176**(2), 26S–38S (1998).
49. J. V. Quinn, *Tissue Adhesives in Wound Care*, B.C. Decker, Inc., Hamilton (1998).
50. J. A. Palero et al., "*In vivo* nonlinear spectral imaging in mouse skin," *Opt. Express* **14**(10), 4395–4402 (2006).
51. P. Martin and S. J. Leibovich, "Inflammatory cells during wound repair: the good, the bad and the ugly," *Trends Cell Biol.* **15**(11), 599–607 (2005).
52. D. G. Greenhalgh, "The role of apoptosis in wound healing," *Int. J. Biochem. Cell Biol.* **30**(9), 1019–1030 (1998).
53. U. K. Saarialho-kere et al., "Distinct localization of collagenase and tissue inhibitor of metalloproteinases expression in wound healing associated with ulcerative pyogenic granuloma," *J. Clin. Invest.* **90**(5), 1952–1957 (1992).
54. D. Greiling and R. A. F. Clark, "Fibronectin provides a conduit for fibroblast transmigration from collagenous stroma into fibrin clot provisional matrix," *J. Cell. Sci.* **110**(7), 861–870 (1997).
55. M. J. Eichler and M. A. Carlson, "Modeling dermal granulation tissue with the linear fibroblast-populated collagen matrix: a comparison with the round matrix model," *J. Dermatol. Sci.* **41**(2), 97–108 (2006).
56. C. Dealey, *The Care of Wounds: A Guide for Nurses*, Wiley-Blackwell, West Sussex (1999).
57. H. P. Lorenz and M. T. Longaker, "Wounds: biology, pathology and management," Chapter 10 in *Surgery: Basic Science and Clinical Evidence*, J. A. Norton, Ed., pp. 191–208, Springer science+Business media, LLC, New York (2008).